Journal of Colloid and Interface Science 678 (2025) 1153–1164

Contents lists available at ScienceDirect

Journal of Colloid And Interface Science

journal homepage: www.elsevier.com/locate/jcis

Regular Article

Enhanced rare earth element recovery with cross-linked glutaraldehyde-lanthanide binding peptides in foam-based separations

Luis E. Ortuno Macias [a,b], Honghu Zhang [c], Benjamin M. Ocko [c], Kathleen J. Stebe [d], Charles Maldarelli [a,b,*], Raymond S. Tu [a,*]

[a] Department of Chemical Engineering, The City College of New York, New York, NY, 10031, USA
[b] The Benjamin Levich Institute for PhysicoChemical Hydrodynamics, The City College of New York, New York, NY, 10031, USA
[c] National Synchrotron Light Source II, Brookhaven National Laboratory, Upton, NY, 11973, USA
[d] Department of Chemical and Biomolecular Engineering, University of Pennsylvania, Philadelphia, PA, 19104, USA

GRAPHICAL ABSTRACT

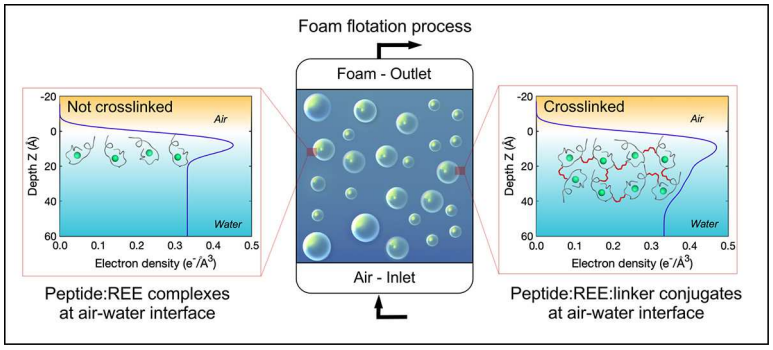

ARTICLE INFO

Keywords:
Rare earth elements
Glutaraldehyde
LBT peptides
Separation
Interface

ABSTRACT

Hypothesis: Lanthanide Binding Tag (LBT) peptides that coordinate selectively with lanthanide ions can be used to replace the energy intensive processes used for the separation of rare earth elements (REEs). These surface-active biomolecules, once selectively complexed with the trivalent REE cations, can adsorb to air/aqueous interfaces of bubbles for foam-based REEs recovery. Glutaraldehyde, an organic compound that is a homobifunctional crosslinker for proteins and peptides, can be used to enhance the adsorption and interfacial stabilization of lanthanide-bound peptides films.

Experiments: The stability of the interfacial cross-linked films was tested by measuring their dilational and shear surface rheological properties. Surface activity of the adsorbed species was analyzed using pendant drop tensiometry, while surface density and molecular arrangement were determined using x-ray reflectivity and x-ray fluorescence near total reflection.

Findings: Glutaraldehyde cross-linked REE-peptide complexes enhance the adsorption of lanthanides to air-water interfaces, resulting in thicker interfacial structures. Subsequently, these thicker layers enhance the dilational and shear interfacial rheological properties. The interfacial film stabilization and REEs extraction promoted by the cross-linker presented in this work provides an approach to integrate glutaraldehyde as a substitute of

* Corresponding authors.
E-mail address: tu@ccny.cuny.edu (R.S. Tu).

https://doi.org/10.1016/j.jcis.2024.08.225
Received 22 June 2024; Received in revised form 25 August 2024; Accepted 26 August 2024
Available online 6 September 2024

common foam stabilizers such as polymers, surfactants, and particles to optimize the recovery of REEs when using biomolecules as extractants.

1. Introduction

Rare earth elements (REEs) comprise the 15 lanthanide elements, along with yttrium and scandium, and are generally divided into two groups based on their physical and chemical properties: heavy REEs (gadolinium to lutetium, Z = 64 to 71; and yttrium), and light REEs (lanthanum to europium, Z = 57 to 63; and scandium) [1–3]. The growth of numerous technologies is driving the demand for these metals. These elements play a crucial role in several applications and are fundamental for the production of powerful magnets, catalysts, and advanced electronics [4–6]. Mining feedstocks recover the REEs as their stable trivalent cation (Ln^{3+}) in aqueous mixtures. The cations are strong Lewis acids forming ionic coordinating complexes with nucleophiles, e.g. water and carboxylate oxygens. Separation from mining feedstocks involves identifying nucleophilic chelating ligands (extractants) which form a coordinating complex specific to a particular lanthanide cation. Liquid-liquid extraction is the established industry method for REE separation of the cations. In this process, synthetic small molecule organic extractants are dissolved in an organic phase and brought into contact with an aqueous phase containing the REEs. The resulting coordinating complex is soluble in the organic phase due to the hydrophobic nature of the extractants. This separation method is weakly selective, requiring multiple stages to achieve satisfactory discrimination, which leads to the consumption of excessive amounts of solvents that have significant environmental impacts [7,8], thus new environmentally sustainable and industrial-suited separation and purification processes are required. Several new sustainable separation processes of REEs are being explored to address environmental concerns associated with traditional methods, such as ionic liquid extraction [9,10], supercritical fluid extraction [11,12], adsorption of metals on organic polymers and MOFs [13,14], and membrane separation [15,16].

Biomolecular extractants have recently gained attention as highly selective “green extractants”, for biodegradable alternatives to traditional chemical reagents in all aqueous separation processes [17–20]. Lanthanide binding tag (LBT) peptides are biomolecular extractants which derive from the calcium-binding protein, calmodulin. LBTs are short molecules (17-20 amino acids) designed to selectively bind to lanthanides cations [21,22]. The high selectivity of these peptides for lanthanides is due to their specific amino acid sequence that provide the chelating nucleophiles, along with the arrangements of other functional groups within this peptide sequence that upon metal complexation creates a highly specific binding environment (a coordinating loop) that preferentially interacts with lanthanide ions over other metals ions. Extraction platforms mediated by LBT peptides have emerged as promising substitutes for traditional recovery and purification methods. In particular, genetic engineering has been utilized to express and display LBTs on the surfaces of microbial cells for the selective separation of REEs [23–27]. These platforms have the advantage of all aqueous chemistry, but excess negative charges on the surface can result in nonspecific electrostatic binding which degrades selectivity, and recovery involves additional centrifugation steps for recovery.

Foam-based separation processes are widely applied in the mineral processing industry for the extraction of valuable minerals [28,29]. We have been developing and studying LBT peptides to extract REEs using a foam-based platform. The LBT^{3-} peptide, with the amino acid sequence YIDTNNDGWYEGNELLA, is a 17 residues peptide with a net charge of -3 in the uncomplexed state at a pH of 6 designed for the selective adsorption of REEs to air-water interfaces [20]. This peptide, selective for Tb^{3+} among the lanthanide cations, can fold and enclose lanthanide cations in solution resulting in the formation of a stable binding pocket through the residues D1, N3, D5, W7, E9, and E12 (see Figs. 1A and 1B).

In previous work, we demonstrated that LBT^{3-}:REE complexes are surface active, retain their binding pocket integrity upon adsorption to air-water interfaces, and the peptide enables the selective interfacial extraction from equimolar mixtures of Tb^{3+} and La^{3+} (with surface selectivity, Tb^{3+}/La^{3+}, of approximately 2 when binding loops are saturated with cations) [20]. We also established that a net charge of -3 (observed at neutral pH) for the unbound peptide was crucial to avoid non-specific binding of excess metal in solution with charged groups not participating in the coordination loop. This prior work was proof-of-concept that LBT^{3-} could be used for interfacial separations of REEs in foam-based processes, but the low surface coverages of peptide-metal complexes and slow dynamic surface tensions relaxations will limit the applicability of this technique. These factors may hinder process efficiency due to the need for higher interfacial activity, more rapid reduction in surface tension, and in particular the need for thicker interfacial layers for optimal foam stability [30–33]. Large molecular weight amphiphiles, such as polyethylene glycols (PEG) conjugated molecules, proteins, and others polymers [28,29,34], are commonly used for the stabilization of foams as they form interfacially thick elastic layers. These could potentially be used as co-surfactants to enhance the foam stability, but co-surfactants can compete with LBT^{3-} molecules for adsorption sites at the air-water interface of bubbles, displacing or preventing the adsorption of the surface active peptides.

Glutaraldehyde (GA) readily reacts with amino groups of proteins and peptides (with higher affinity for ϵ-amino and α-amino groups) in a wide pH range and under mild conditions forming stable crosslinks [35]. In addition to the high stability of cross-linking through covalent bonds between amino groups, glutaraldehyde is the most widely used crosslinking agent due to its low cost, high reactivity, and ability to stabilize matrices in various applications [35,36]. Since cross-linking with peptides is expected to occur in solution and not at the surface, glutaraldehyde can potentially be used not as co-surfactant, but as a “facilitating agent” that promotes the adsorption of larger molecular weight metal-peptide complexes to air-water interfaces.

In this study, we exploit the high reactivity of glutaraldehyde for peptides to promote the formation of metal-peptide-GA complexes in solution that diffuse to the air-water interface, resulting in a greater adsorption/extraction of metals (see Fig. 1C). Moreover, once adsorbed to the surface, these complexes can form interfacial networks, as depicted in Fig. 1C, which enhances the elastic properties of the surface films. The improved rheological properties are crucial for the formation and stabilization of foams, as it provides the surface layer with greater resistance to deformation and rupture.

The surface activity of metal-peptide-GA is probed by pendant drop tensiometry (PDT) to confirm the enhancement of the adsorption of species by glutaraldehyde. The stability of the interfacial films induced by the cross-linker is characterized by measuring the dilational and shear surface rheological properties. Solution phase characterization of structures is performed by using transmission electron microscopy (TEM) imaging, dynamic light scattering (DLS), and zeta potential measurements. Detailed characterization of the molecular composition and arrangements at the interface is achieved through x-ray interrogation of adsorbed films using x-ray reflectivity (XR) and x-ray fluorescence near total reflection (XFNTR).

These surface molecular measurements reveal the enhanced adsorption of lanthanides and peptides, along with the formation of thicker layers at the air-water interface with elevated interfacial elasticity, which contribute to the improved stability of the surface films. Importantly, we demonstrate that GA does not significantly alter the surface affinity and selectivity of lanthanide-peptide complexes. Thus, we show that glutaraldehyde can act as a “facilitating agent” for the enhanced

(A)

	Position																
NT	Y	I	D	T	N	N	D	G	W	Y	E	G	N	E	L	L	A	CT
NH_3^+-	-1	0	1	2	3	4	5	6	7	8	9	10	11	12	13	14	15	-$CONH_2$

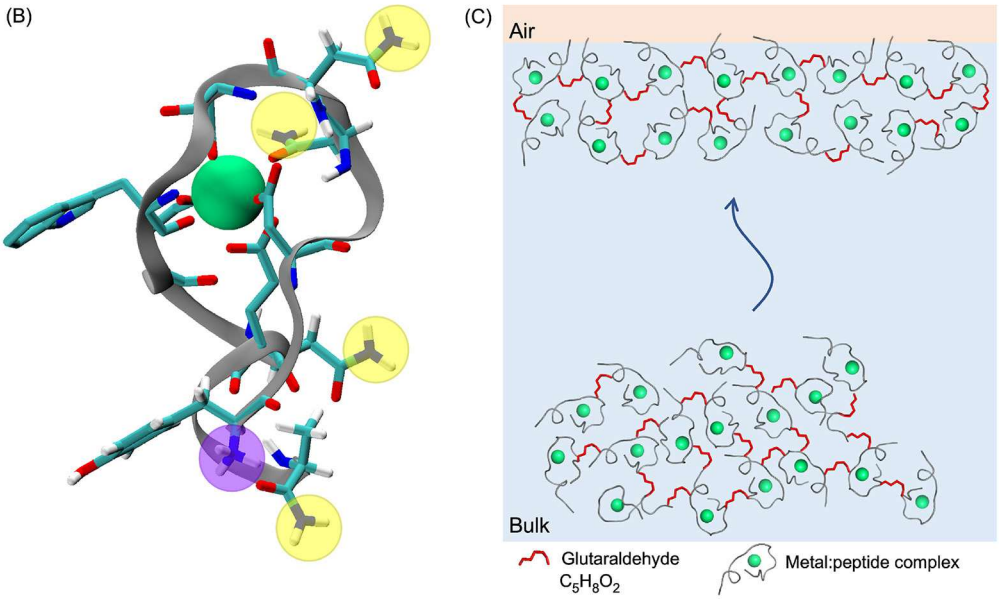

Fig. 1. (A) Sequence alignment of LBT^{3-}, with amino acids coordinating with the cations colored in red. NT and CT are the N-terminus and C-terminus respectively, with charges corresponding to the experimental conditions (pH 6). (B) Molecular dynamic simulations snapshot of one of the stable peptide-Tb^{3+} conformations [20] with NH_2 groups from asparagine residues and the C-terminus highlighted in yellow and $(NH_3)^+$ from the N-terminus of the peptide highlighted in purple. (C) Schematic representation of hypothesized cross-linking of metal-peptide complexes in solution by glutaraldehyde and further diffusion of linked-complexes to the air-water interface.

surface adsorption and separation of these metals, enabling selective separation of rare earth elements. The cross-linking of metal-peptide complexes in solution using glutaraldehyde, which enhances the efficiency of rare earth element separation, advances our understanding of optimizing intermolecular interactions in solution, interfacial interactions, and film stabilization through chemical linkage of peptides that form nanometer-sized structures. This work significantly contributes to broader knowledge in colloid and interface science, particularly in the designing materials with tailored properties for REE separation.

2. Materials and methods

Materials LBT^{3-}: YIDTNNDGWYEGNELLA (purity ≥95%) labeled at the N-terminus with a free amine and at the C-terminus with an amide, was purchased from GenScript (Piscataway, NJ, USA), diluted to a stock concentration of 300 μM in buffer solutions containing 100 mM of NaCl (purity ≥99.5%, Sigma-Aldrich) and 50 mM of MES (purity ≥99.5%, Sigma-Aldrich) at a pH of 6, and used without additional purification. $TbCl_3$ hexahydrate (purity ≥99.999%), $LaCl_3$ heptahydrate (purity ≥99.999%), and glutaraldehyde solution (50 wt.% in H_2O) were purchased from Sigma-Aldrich and diluted to a stock concentration of 25 mM for the metal salts and 20 mM for glutaraldehyde, in the same buffer solution containing 100 mM of NaCl and 50 mM of MES. Buffer solution is filtered using a 0.22 μm polytetrafluoroethylene filter. Ultrapure water is obtained from a Milli-Q water filtration unit (EMD Millipore) with a resistivity of 18.2 MΩ-cm and used for preparation of buffer solution.

Cross-Linking of Lanthanide:LBT^{3-} Complexes with Glutaraldehyde Solutions containing peptide and cations were first prepared, then reacted with glutaraldehyde by adding different volumes of a stock solutions of 20 mM and 50 mM of the cross-linker (with glutaraldehyde solutions prepared in the same buffer used for the peptide and lanthanides stock solutions). After the addition of glutaraldehyde, the solutions were left to sit undisturbed for a minimum of 40 hours at 4 °C before surface and bulk measurements.

Surface Tension Measurements Dynamic surface tensions at the air/aqueous interface were measured using a pendant drop tensiometer (Attension Theta, Biolin Scientific). Solutions were prepared with 100 μM of LBT^{3-} peptide, 400 μM of Tb^{3+}, and different concentrations of glutaraldehyde and 16 μL drops of these solutions were formed and suspended from a 16-gauge metal needle. An optical train forms images of the silhouette of the hanging drop which are captured by a camera; fitting of the drop contour with solutions of the Young Laplace equation allows the surface tension of the drop to be calculated. The drop is formed impulsively and the peptide or different complexes adsorb to the clean surface; images of this process captured over time measure the dynamic tension.

Interfacial Dilational Rheology Dilational rheology measurements are undertaken using a pendant drop tensiometer (Attension Theta, Biolin Scientific). Solutions were prepared with 100 μM of LBT^{3-} peptide, 400 μM of Tb^{3+}, and different concentrations of glutaraldehyde and 16 μL drops of these solutions were formed and suspended from a 16-gauge metal needle. Once the solutions reached a quasi-equilibrium adsorption state (using dynamic surface tension measurements as a guide), the surface tension response $\gamma(t)$ to controlled sinusoidal perturbations (small amplitude) of the drop area $A(t)$ at frequencies (f) of 0.05-0.1 Hz ($\omega = 2\pi f$) was recorded [37].

$$A(t) = A_o + \Delta A \sin \omega t \tag{1}$$

$$\gamma(t) = \gamma_0 + \Delta\gamma \sin(\omega t + \delta) \tag{2}$$

$$\bar{E}^2 = E'^2 + E''^2 \tag{3}$$

$$E' = E \cos\delta \tag{4}$$

$$E'' = E \sin\delta \tag{5}$$

where A_0 is the initial interfacial area, ΔA the amplitude of the area oscillations, ω is the oscillation frequency, γ_0 the reference surface tension, $\Delta\gamma$ the amplitude of the surface tension oscillations, δ is the phase angle (measure of the lag between the applied surface deformation and the resultant surface tension response), t represents time, and E' and E'' are the dilational (linear) elastic or storage modulus and viscous or loss modulus. All experiments were conducted with a $\Delta A/A_0$ value of 0.017.

Interfacial Shear Rheology Surface shear rheology of interfacial layers adsorbed from solutions containing 100 μM LBT^{3-} peptide, 400 μM of Tb^{3+} and different concentrations of glutaraldehyde were measured by a Physica MCR 702e stress-controlled Rheometer (Anton Paar) with a measuring body of a biconical geometry (68 mm, 2 x 5°) with sharp edges. Prior to measurements, 14 mL of solution was poured into the sample holder, and then the bicone was positioned at the surface by a normal force assisted surface detection of the air-water interface. Once the solutions reached a quasi-equilibrium adsorption state (using dynamic surface tension measurements as a guide), dynamic frequency sweeps were executed with a strain amplitude of 0.03% at frequencies (f) of 0.1-10 Hz ($\omega = 2\pi f$) to measure the shear elastic (G′) and viscous (G″) moduli after the contribution of the sub-phase subtracted [38].

Dynamic Light Scattering (DLS) DLS was performed on a Zetasizer Nano ZS (Malvern). 1 mL of the different solutions of peptide or metal:peptide complexes at different cation concentrations and a fixed concentration of LBT^{3-} of 100 μM, were analyzed in plastic cuvettes at 25 °C. The z-average diameter and polydispersity index (PDI) were calculated from a cumulants analysis, where the diffusion coefficient of particles is converted into a particle size by using the Stokes-Einstein equation.

Zeta Potential Zeta potential measurements were taken using a Zetasizer Nano ZS (Malvern). 700 μL of the different solutions of peptide or peptide and lanthanides at different cation concentrations and a fixed concentration of LBT^{3-} of 100 μM, were loaded in folded capillary cells and analyzed at a temperature of 25 °C. Electrophoresis measurements were calculated based on the movement of the particles under the influence of an applied electric filed relative to the liquid in which they are suspended. Zeta potential measurements were then computed by using the Henry equation for the electrophoretic mobility, under conditions where the Debye length (1/k) is small compared to the particle radius (a) (Smoluchowski limit, F(ka) = 1.5).

Transmission Electron Microscopy (TEM) TEM measurements were undertaken on a Tecnai Spirit TWIN TEM electron microscope operated at an accelerating voltage of 120 kV. Solutions were prepared with 100 μM LBT^{3-} peptide, 400 μM of lanthanide and different concentrations of glutaraldehyde and 4 μL of samples were deposited onto TEM grids (pure carbon on copper mesh, Ted Pella Inc., USA) that were previously treated with a plasma cleaner (Fischione M1070 NanoClean) for 60 seconds. The sample on the grid was lightly blotted with filter paper, and then stained with 2% uranyl acetate solution and blotted once again. The sample was rinsed with water and the excess solution was removed by blotting the edge of the grid with filter paper.

Liquid Surface X-ray Measurements X-ray reflectivity (XR) and x-ray fluorescence near total reflection (XFNTR) were measured at the Open Platform and Liquid Scattering (OPLS) end station of the Soft Matter Interfaces beamline (SMI, 12-ID) at the National Synchrotron Light Source II, Brookhaven National Laboratory. The liquid samples were placed in troughs of maximum surface area of 40.3 cm^2. The troughs were filled with approximately 18 mL of different solutions containing LBT^{3-} peptide, lanthanide cations, and glutaraldehyde. The troughs were contained in a sealed aluminum box, resting on a vibration isolation table. After the troughs were filled, the box was closed. A slight overpressure of water-saturated helium was kept in the box to reduce x-ray background scattering. All measurements were taken after the adsorption of molecules to the air-water interface reached a near-constant surface tension (according to surface tension measurements obtained in the pendant drop experiments) and at room temperature.

X-ray Reflectivity (XR) XR measures the interfacial electron density profile. X-ray reflectivity data were measured as a function of wave vector transfer $Q_z = (4\pi/\lambda)\sin(\alpha)$ along the surface normal to cover the range 0.016 $Å^{-1} < Q_z < 0.6$ $Å^{-1}$, where α is the angle of incidence and λ is the x-ray wavelength $\lambda = 1.28$ Å. XR data was measured with an area detector and measured multiple times to check for stability. XR measurements were fit to a model functional form to compute the electron density $\rho(z)$ along the z direction perpendicular to the interface, and averaged over the $x-y$ plane of the surface, with the model function represented by a sum of error functions [39]:

$$\rho(z) = \frac{1}{2}\sum_{i=0}^{N-1} \mathrm{erf}\left(\frac{z - z_i}{\sqrt{2}\sigma}\right)(\rho_i - \rho_{i+1}) + \frac{\rho_0 - \rho_N}{2} \quad (6)$$

with $\mathrm{erf}(z) = (2/\sqrt{\pi})\int_0^z e^{-t^2}dt$; N the number of internal interfaces within the surface film, σ the interfacial roughness, ρ_0 the electron density of the bulk aqueous phase, ρ_N the electron density of the air phase, ρ_i and z_i the electron density and the position of the i^{th} slab and interface, respectively. The thickness of the i^{th} slab, d_i, is defined as $|z - z_i|$. X-ray reflectivity was computed using the Parratt formalism by discretizing the electron density profile (EDP) from equation (6). XR measurements were normalized to the Fresnel reflectivity R_F, which is calculated for a theoretical liquid-air interface where the electron density varies as a step function between the two bulk phases [39].

X-ray Fluorescence Near Total Reflection (XFNTR) XFNTR measures the surface number density of fluorescing metal ions (number per $Å^2$). X-ray fluorescence intensity was measured for a range of Q_z near the critical value Q_c for total reflection. The x-ray fluorescence spectrum was measured by a Vortex EX90 silicon drift detector placed above the interface and spectra were normalized to the incident beam intensity. The XFNTR signal was obtained by integrating the fluorescence peak of lanthanide cations over the acceptance volume in the aqueous phase to obtain the surface concentration, as described in detail in the Supplementary Information and in previous work [40,41].

3. Results and discussion

Bulk Aggregation of LBT^{3-}:Tb^{3+} and Effect of GA Cross-linking. We examine the Tb^{3+}-induced association of LBT^{3-} peptides and the cross-linking of cation-peptide complexes. Morphological changes of the biomolecular aggregation due to ion complexation with Tb^{3+} cations are discussed first, followed by cross-linking with glutaraldehyde.

Fig. 2A shows DLS measurements of the z-average hydrodynamic diameter of species in solution for samples containing peptide at 100 μM and different concentrations of Tb^{3+} cations. These values are derived from the number size distributions (refer to **Fig. S1**), which are obtained from the intensity distribution using scattering theory. The error bars reported represent the width of the peaks from the number size distribution (standard deviation), indicating the distribution of the peak (**Fig. S1**). In the absence of trivalent cations, species with hydrodynamic diameter of 0.7 ± 0.1 nm are observed, indicating the presence of only monomers in solution. This monomeric state at a pH of 6 is expected, since carboxyl groups on the side chains of the molecule are negatively charged (with a total net charge of -3 for one peptide in the uncomplexed state), providing repulsive effects that counteract aggregation. As the concentration of Tb^{3+} is increased to match the peptide concentration to 100 μM, DLS reveals the existence of structures similar in size to those observed with single unassociated peptides, which indicates the presence of metal-peptide complexes in the solution. With

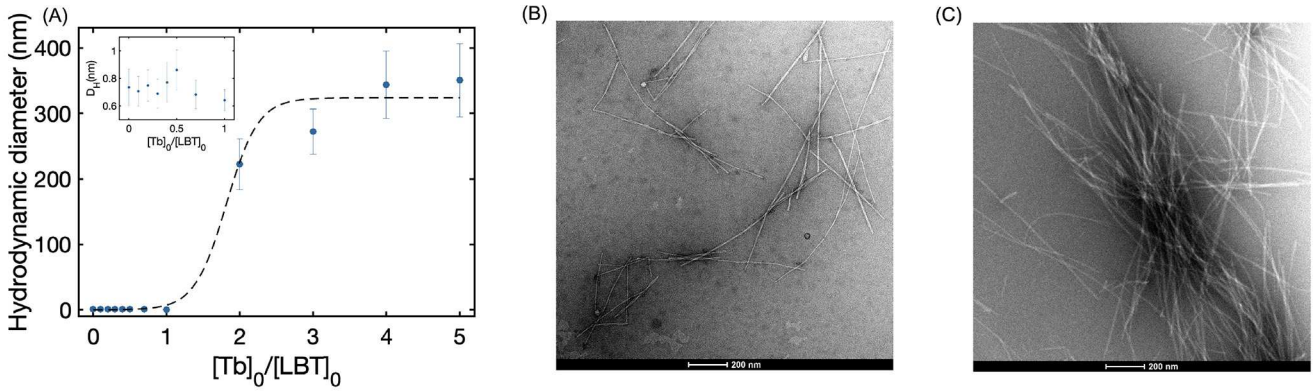

Fig. 2. (A) Average hydrodynamic diameter (D_H) from the number-based distribution for solutions containing 100 μM of LBT^{3-} peptide and different concentrations of Tb^{3+} cations. The data was modeled using a sigmoidal function, represented by the dashed curve, to enhance visualization. The inset plot contains the data for undersaturated regimes $[Tb]_0 \leq [LBT^{3-}]_0$. (B) Dry TEM image from a solution containing 100 μM of LBT^{3-} peptide with 400 μM of Tb^{3+} cations. (C) Dry TEM image from a solution containing 100 μM of LBT^{3-} peptide, 400 μM of Tb^{3+} cations and 1 mM of glutaraldehyde.

excess Tb^{3+} cations (cations concentration sufficient to saturate the peptide), DLS measurements shows evidence of structures that have larger hydrodynamic diameter (344 ± 51 nm for 400 μM of Tb^{3+}), suggesting that the trivalent cations cause the formation of these aggregates. Self-assembly structures of peptides has been observed with multivalent cations in solution, and association is generally attributed to ionic bridging, counterion screening of charges, and hydrophobic interactions [42–44]. The formation of nanometer-sized structures was only observed under conditions in which the peptide is oversaturated with Tb^{3+} (see Fig. 2A), which indicates that total neutralization of charges play an important role in aggregation. Note that the intensity-based size distribution also indicates structures exhibiting larger hydrodynamic diameters and monomers (with monomer having the same size as those reported in the number distribution). This was only observed for Tb^{3+} concentrations lower than that of the peptide (data not shown). While this suggests the existence of aggregates in an undersaturated regime, potentially arising from bound peptides already aggregating at these low Tb^{3+} concentrations, their proportion in solution remains small compared to the monomeric form.

To provide direct experimental evidence of the charge effect in the association upon metal binding, zeta potential measurements of uncomplexed peptide and Tb^{3+}-complexed peptide (at the concentration of cations where aggregate structures are observed), were taken. While the negative surface charge of LBT^{3-} in the uncomplexed state (-14 ± 1 mV) is consistent with the negatively net charge of the peptide at a pH of 6; in the presence of excess Tb^{3+}, a zeta-potential of -0.06 ± 0.01 mV was obtained, which suggests aggregate formation requires the joint effects of charge neutralization and metal-induced conformational changes on the peptide structure. The presence of nanometer-sized structures was confirmed by TEM, and are shown in Fig. 2B. These appear as fibrillar structures of diameter approximately 6 nm, with lengths in agreement with the hydrodynamic diameters obtained by DLS (approximately 200-400 nm), although larger lengths are observed.

Fig. 2C shows the resulting metal-peptide structures after 48 hours of incubation with the cross-linker. GA was added to a solution containing LBT^{3-} and Tb^{3+}, at a concentration of 100 μM of peptide, 400 μM of trivalent cations, and 1 mM of the cross-linker. In the presence of glutaraldehyde, well-organized fibers are still observed, with lengths of fibrils of similar size to the non-linked fibrils but diameters of approximately 11 nm. These thicker fibrils suggest that glutaraldehyde might act as a connector between two already formed and well-ordered structures, and each cross-linker molecule react with a specific amine group expose to the solvent. Moreover, we hypothesize that the cross-linker does not significantly disturb the Tb^{3+}-bound conformation of the peptide, because the highly organized fibers remain in the glutaraldehyde-associated state.

While LBT^{3-} contains amides on the side chain of the amino acid asparagine and at the C-terminus (yellow circled groups in Fig. 1B) that can react with glutaraldehyde, the reaction is highly efficient with the primary amine located at the N-terminus of the peptide (purple circled group in Fig. 1B). Hence, in order for fibrils to preserve the observed highly-ordered organization upon cross-linking, glutaraldehyde is most likely to react with only the $-(NH_3)^+$ at the N-terminus of the peptide. This preference is potentially due to two reasons: (1) highly reactivity of glutaraldehyde for primary amine over amide groups [35], and (2) well-ordered fibrils formed upon Tb^{3+}-binding expose $-NH_3^+$ groups at the N-terminus of the peptide to the solvent.

Surface Tension of Adsorbed Layers of LBT^{3-}:Tb^{3+}:GA. The surface tensions of interfacial layers formed by adsorption from solutions containing different mixtures of LBT^{3-}, Tb^{3+}, and glutaraldehyde were measured using the pendant drop technique. Terbium was selected for studying the adsorption of cross-linked metal-peptide conjugates because Tb^{3+} is the lanthanide to which the peptide has the highest affinity. All solutions were observed to reduce the surface tension with time (**see Fig. S2** for dynamic surface tension), creating interfacial layers of increasing surface concentration over time. In this work, we report the quasi-equilibrium surface tension, as the value following a 1-hour adsorption period from the solution, after which a gradual and minimal decrease in tension over time was observed for the peptide concentration (100 μM) studied. We identified these values as quasi-equilibrium (slow reduction in surface tension). The quasi-equilibrium behavior is due to the slow adsorption of peptide as the interface becomes saturated and the slow rearrangement on the surface of the molecules occurs to reposition hydrophobic groups into the air phase. The quasi-equilibrium tensions were first measured for solutions containing a fixed value of LBT^{3-}, Tb^{3+} cations (100 μM for the peptide and 400 μM for the trivalent cations), and increasing concentrations of GA, and reported in Fig. 3B. A tension of 72.8 mN/m for a clean interface from a solution containing 100 mM of NaCl and 50 mM of MES buffer at a pH of 6 is recorded. Fig. 3B shows that introducing glutaraldehyde into solutions containing LBT^{3-}:Tb^{3+} complexes and further increasing GA's concentration results in lower surface tension values. The greater reduction in surface tension for higher concentration of glutaraldehyde might be the result of one or the combination of the two following events: (1) a greater concentration of non-linked/unreacted glutaraldehyde molecules adsorbed to the air-water interface, and (2) a greater population of cross-linked Tb^{3+}-peptide-GA adsorbed to the air-water interface because more Tb^{3+}-peptide are interconnected due to higher density of cross-linking in solution. The second scenario is supported by the quasi-equilibrium surface tension values obtained from a solution containing 1 mM of GA, and a solution containing 1 mM of GA

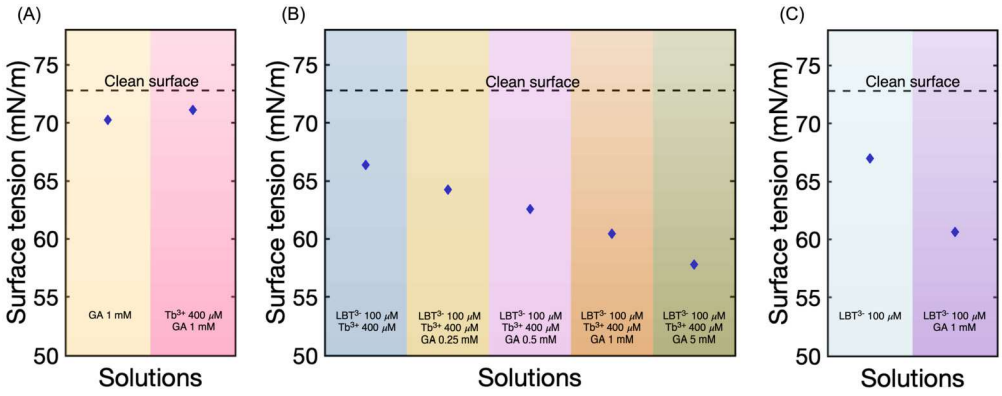

Fig. 3. Quasi-equilibrium surface tension measurements for (A) 1 mM of glutaraldehyde, and 400 μM of Tb^{3+} cations with 1 mM of glutaraldehyde; (B) mixtures of 100 μM of LBT^{3-}, 400 μM of Tb^{3+} cations, and different concentrations of glutaraldehyde; and (C) 100 μM of LBT^{3-}, and 100 μM of LBT^{3-} with 1 mM of glutaraldehyde.

and 400 μM of Tb^{3+} cations, reported in Fig. 3A. Quasi-equilibrium tension from these solutions are above 10 mN/m of the values reported from solutions containing peptides, which indicates that glutaraldehyde is not significantly surface active to reduce the surface tension to values of 64 mN/m and below, presented in Fig. 3B for those solutions containing peptide. The decrease in tension with increase in the concentration of the GA cross-linker suggests that the cross-linked conjugates (LBT^{3-}:Tb^{3+}:GA) form a more well-packed, crowded interfacial layer of higher surface concentration (lower tension) relative to the case where the conjugates are not cross-linked, suggesting that the cross-linked species has a more compact molecular conformation which allows for the higher surface concentration. In this regard, the effect of cross-linking on adsorption behavior is similar to the influence of cross-linking on the adsorption of water soluble, surface active polymers at the oil-water interface as studied by Bochenek et al. [45]. In their study of the adsorption of poly(N-isopropylacrylamide, pNIPAM) from the aqueous phase to the oil-water interface in a Langmuir trough, the star-shaped pNIPAM polymer, upon compression, formed a more condensed layer than the linear pNIPAM, and cross-linked pNIPAM polymers forming microgels give rise to even more condensed layers.

Quasi-equilibrium surface tension of unbound peptide in the absence and presence (1 mM) of glutaraldehyde, are presented in Fig. 3C. As for the non-linked peptide and non-linked metal-peptide, the quasi-equilibrium surface tension for the cross-linked peptide and cross-linked metal-peptide complexes are almost identical; indicating that the cross-linking in solution and adsorption of molecules to the air-water interface is similar for the uncomplexed and Tb^{3+}-complexed peptide when glutaraldehyde is in solution at the same concentration. Note that the glutaraldehyde cross-linked peptide, whether in the metal-complexed or uncomplexed state, is more surface active than the non-linked peptide, and this is independent of its complexation with Tb^{3+} (Figs. 3B and 3C). Moreover, this also applies to the dynamic surface tension, as shown in **Figs. S2A** and **S2B**.

Dynamic surface tensions for solutions containing a fixed value of LBT^{3-} and Tb^{3+} cations (100 μM for the peptide and 400 μM for the trivalent cations) reported in **Fig. S2A**, indicate that the reduction in tension within the first 10 seconds becomes greater as the concentration of glutaraldehyde in solution is increased, with the greatest reduction value for a bulk concentration of GA of 5 mM (15% reduction compared with the surface tension of a clean interface, and after 8 seconds of forming the pendant droplet). This rapid reduction in surface tension is of significant importance in foam-based separation processes because molecules are able to populate the interface rapidly and prevent bubble coalescence. Moreover, a faster population of the interface is of significant importance for packing gas/air surfaces when foams are formed in liquid. Interfacial rheology measurements of surface viscoelasticity provide details of the stability of the interfacial films in the presence of glutaraldehyde.

Rheological Properties of LBT^{3-}:Tb^{3+}:GA Films at the Air-Water Interface. The interfacial dilational and shear rheology measurements are taken as a measure of stability of adsorbed layers of peptides-metal-glutaraldehyde complexes. External perturbations can produce internal relaxation of the adsorbed layers, and this behavior provides useful insight on the mechanics of the adsorbed layers and the stability of the foam in a foam fractionation separation process. The dilational rheology of interfacial layers adsorbed from solutions containing Tb^{3+}:peptide complexes and different concentration of glutaraldehyde are measured. Deformation of the interfacial layer in a quasi-equilibrium state was induced by increasing and decreasing the area of the liquid surface while still retaining a pendant form. The |E| values, shown in **Fig. S3**, indicate a stronger rheological response due to the cross-linking of LBT^{3-}:Tb^{3+} complexes with glutaraldehyde. For all the studied solutions, the storage component (E′) of the dilational viscoelasticity was higher than the loss component (E″), indicating that all interfacial films exhibit an elastic solid-like behavior at the frequencies studied here (Fig. 4A and **Fig. S4A**). Moreover, the E′ increases gradually with the increase of the oscillation frequency, which can be attributed to the reorganization of the interfacial molecular arrangement. More precisely, for low oscillation frequencies, molecules at the interface have longer time to adapt to the area change, which results in a lower E′ as the entanglement relaxes. While, when the oscillation frequency is increased, molecules populating the interface have less time to adapt to the deformation of the interface and hence greater dilational moduli are observed.

The layer formed from a solution containing no glutaraldehyde (only peptide and Tb^{3+} cations), has lower values of dilational elasticity and negligible values of dilational viscosity. This might be the result of weak intermolecular interactions in the interfacial adsorbed layer. Fig. 4A shows that the dilational elasticity increases with increasing bulk concentration of glutaraldehyde. The larger surface elastic values are most likely the result of the cross-linking of the film. Hence, a higher concentration of glutaraldehyde in bulk solution provides linkages at the surface caused by a greater population of cross-linked LBT:Tb^{3+}:GA molecules and/or an enhanced cross-linking provided by glutaraldehyde. Interestingly, solutions with bulk concentrations of glutaraldehyde of 1 mM and 5 mM formed interfacial layers with the same dilational elasticity (see **Fig. S4A** for other concentrations of glutaraldehyde).

We hypothesize that for concentrations of GA of 1 mM and higher, cross-linking of metal-peptide complexes by glutaraldehyde begins to saturate leading to only a small increase in the bulk concentration of the LBT^{3-}:Tb^{3+}:GA conjugates and only a marginal increase in surface crowding. As a result, there is no change in the dilatational elasticity of

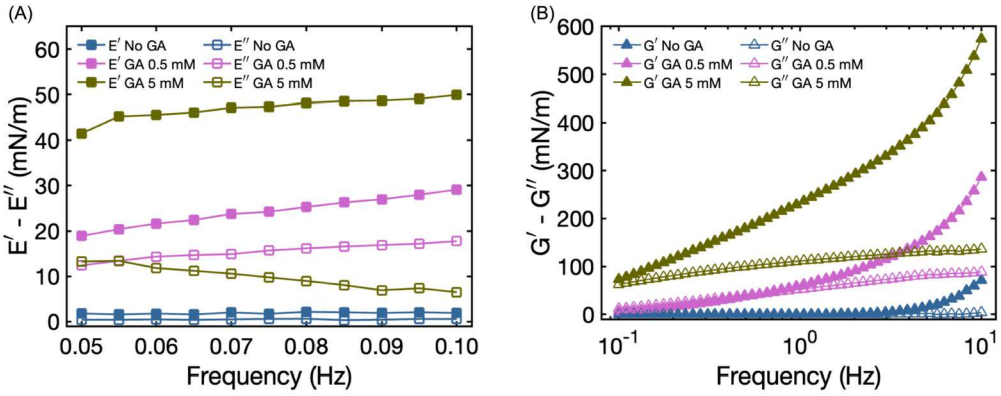

Fig. 4. (A) Dilational and (B) shear rheological surface viscoelasticity for solutions containing 100 μM of LBT^{3-}, 400 μM of Tb^{3+} cations, and different concentrations of glutaraldehyde. Lines are added to enhance the visualization of the trend of values across the studied oscillation frequencies.

the adsorbed surface film. However, as the GA concentration increases from 1 to 5 mM, unreacted glutaraldehyde in the bulk may also co-adsorb to the surface and coexist with LBT^{3-}:Tb^{3+}:GA conjugates. While this does not impact the surface dilatational elasticity, the intercalated smaller free GA molecules induce the observed reduction in the dilatational viscosity E″ by making the surface film less viscous.

Glutaraldehyde can also enhance the dilational viscosity of metal-peptide films adsorbed from bulk to the air-water interface, as seen in Fig. 4A. The increase in surface dilational viscosity provided by glutaraldehyde, which is associated with foamability (formation of foams), strengths the capacity of the layer to adapt deformations, which is of significant importance in a foam-based separation process. Similarly to E′, for solutions containing GA concentrations of 0.25 mM and 0.5 mM, E″ increases as the oscillation frequency increases. The cause of this trend is the same as the behavior observed for the dilational surface elasticity (see **Fig. S4A** for other concentrations of glutaraldehyde). However, for bulk concentrations of GA of 1 mM and 5 mM the dilational viscosity decreases as the oscillation frequency increases. This seems to be consistent with the maximum response of the interfacial layer to dilational stress achieved at 1 mM of glutaraldehyde. When the film reaches its greatest solid-like behavior (no changes in E′ for concentration of GA higher than 1 mM, see Fig. 4A), molecules at the surface might reorganize faster within this rigid structure, as oscillation frequency increase and the times are shorter for restoration.

Surface dilational viscoelasticity measurements were taken for solutions containing 100 μM of peptide alone and 100 μM of peptide with 1 mM of glutaraldehyde, as reported in **Fig. S5A**. In contrast to the effect observed with Tb^{3+}-bound peptides, glutaraldehyde induces a reduction in the elastic (storage) component of the dilational viscoelasticity in films of uncomplexed peptides adsorbed to the air-water interface. This is surprising. The cross-linking of the (unconjugated) LBT^{3-} should lead to a more compact molecular structure in the bulk, and a more crowded surface on adsorption with a larger elasticity. This was observed for the conjugated LBT^{3-}:Tb^{3+} and resulted in the higher elasticity with increase in GA. However, the unconjugated form is charged, and a significant increase in surface concentration on cross-linking LBT^{3-} in the bulk cannot result in a commensurate increase in surface crowding – even with a more compact form for the LBT^{3+}:GA cross-linked peptide – because of the electrostatic repulsion.

The strong effect of electrostatics is observed when comparing the surface dilational viscoelasticity of uncomplexed peptides with those bound to Tb^{3+} (see **Fig. S5B**). When the negatively charged peptides coordinate with cations, their electrostatic charges are neutralized, reducing the repulsive interactions between them. This neutralization diminishes the dilational response of the interface.

Shear viscoelasticity measurements from solutions containing Tb^{3+}:peptide complexes and different concentrations of glutaraldehyde were taken by applying external perturbations to the interfacial layers in a quasi-equilibrium state (Fig. 4B). These measurements are useful to determine the long-term stability of foams, as the shear elastic moduli (G′) correlates with drainage. Similar to the dilational response, weak intermolecular interactions at the surface in the absence of glutaraldehyde result in low values of interfacial shear elasticity G′ and interfacial shear viscosity G″. Moreover, both G′ and G″ increase as the bulk concentration of glutaraldehyde increases, in agreement with the surface dilational viscoelasticity measurements and supporting that in the presence of the cross-linker a stronger interfacial viscoelastic structure at the interface is obtained. For bulk concentrations of glutaraldehyde of 0.25 mM, 0.5 mM, and 1 mM, the viscous modulus dominates (G″ > G′) in the lower oscillation frequency range (see inset in **Fig. S4B**), while in the higher oscillation frequency range (1 Hz - 10 Hz), the elastic modulus surpasses the viscous one (G′ > G″). Thus, these interfacial films have a viscous-like behavior at lower oscillation frequencies and an elastic-like behavior at higher oscillation frequencies, with crossover frequency decreasing as the concentration of glutaraldehyde increases, which correspond to longer relaxation times and implies that the interface is more closely packed as the concentration of glutaraldehyde increases. For the highest bulk concentration of glutaraldehyde (5 mM), the response of the interfacial layer to shear stress is completely elastic for the whole range of oscillation frequencies studied here (see Fig. 4B and inset in **Fig. S4B**).

Hydrodynamic forces such as drag, buoyancy, lift, and pressure gradient forces might influence how these linked complexes organize, orient, and interact at the interface, potentially altering the overall stability and function of the system. These instabilities could lead to localized desorption or rearrangement of the linked complexes, impacting the uniformity of the surface layer. The dilational and shear rheology measurements presented in this work provide critical insights into how these cross-linked metal-peptide conjugate layers respond to dynamic conditions, revealing the stability of the linked conjugates, even under hydrodynamic forces that can affect the architecture of these interfacial networks.

Moreover, compression isotherms can provide information on the stability and packing of the interfacial layers under higher degrees of deformation compared to those studied in dilational and shear viscoelasticity measurements. **Fig. S6** shows the compression isotherms (surface pressure as a function of surface area) of films adsorbed from solutions containing 100 μM of peptide, 400 μM of Tb^{3+}, and different concentrations of glutaraldehyde. These curves were obtained by slowly reducing the volume of the pendant drop (compressing the surface) after quasi-equilibrium adsorption was achieved and stopping the measurement at a point where a pendant drop was still observed to assure accuracy. The isotherms indicate that as the concentration of glutaraldehyde in solution increases, the disappearance of the inflection observed in the isotherm corresponding to the solution without glutaraldehyde becomes

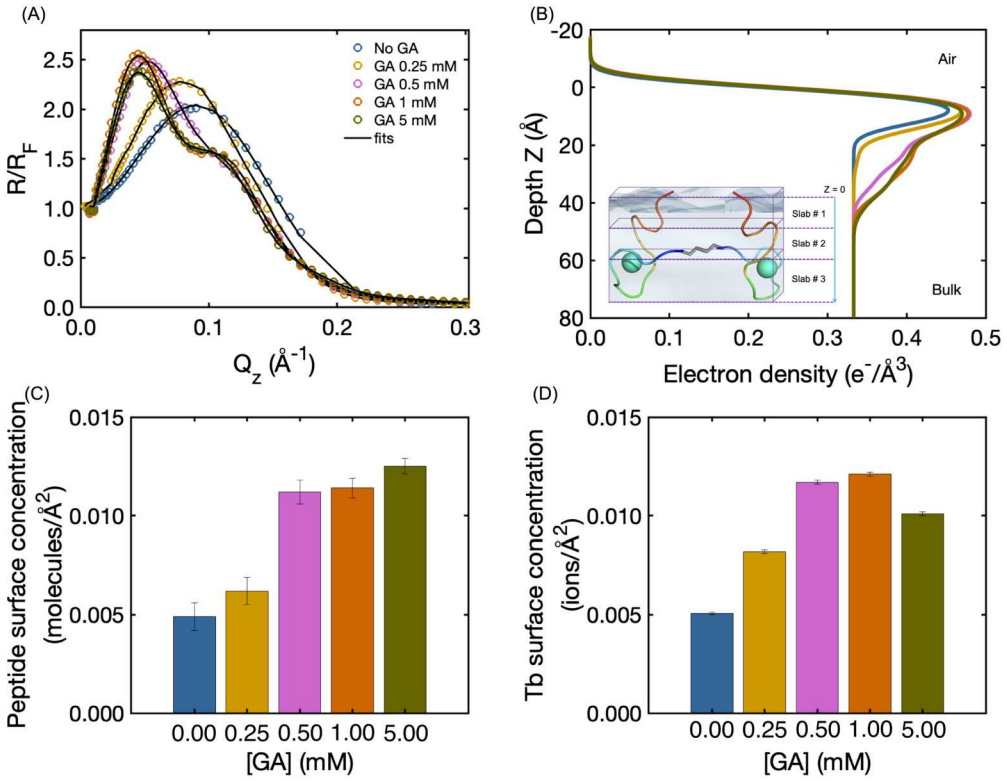

Fig. 5. (A) Normalized reflectivity ($\mathcal{R}/\mathcal{R}_F$) as a function of Q_z normal to the surface for interfacial layers from solutions containing 100 μM of LBT^{3-}, 400 μM of Tb^{3+} cations, and different concentrations of glutaraldehyde. (B) Corresponding electron density profiles of the interfacial layers from Parratt modeling for surface films from solutions containing 100 μM of LBT^{3-}, 400 μM of Tb^{3+} cations, and different concentrations of glutaraldehyde (Inset shows a schematic illustration of the slab model used to fit the reflectivity data for molecules adsorbed at the air-aqueous interface. The model shows a system containing covalently linked metal-peptide-GA conjugates, but the same model was used for all the samples studied with different number of slabs used for each case). Interfacial concentration of LBT^{3-} peptide (C) and Tb^{3+} cations (D) from solutions containing 100 μM of LBT^{3-}, 400 μM of Tb^{3+} cations, and different concentrations of glutaraldehyde. Legend for all plots goes as follow, blue: no GA, yellow: GA 0.25 mM, pink: GA 0.5 mM, orange: GA 1 mM, green: GA 5 mM, black: fits.

more pronounced, indicating a more packed layer under cross-link conditions. As the concentration of glutaraldehyde increases, a steep slope develops, indicating that cross-linking creates a rigid, less compressible film and suggests strong cohesive interactions between molecules and a stable architecture under surface deformation. Additionally, film collapse is not observed under a significant reduction of area (75% reduction), indicating the absence of desorption or multilayer formation at the air-water interface, and providing insight into the architecture of the layers under hydrodynamic forces.

XR/XFNTR Measurements of Adsorbed Layers of LBT^{3-}:Tb^{3+}:GA. The surface concentration of LBT^{3-} peptides adsorbed from solution to an air-water interface were obtained by directing x-rays at grazing incidence to the planar interface of liquid layers of different LBT^{3-}:Tb^{3+}:GA solutions contained in rectangular troughs (depths of a few millimeters), and recording the intensity of the specular reflection ($\mathcal{R}$) at different incident angles (α) (see **Methods**). The specular reflection normalized to the Fresnel reflectivity $\mathcal{R}_F$, ($\mathcal{R}/\mathcal{R}_F$) as a function of the wave vector transfer $Q_z = (4\pi/\lambda)sin(\alpha)$ is fit to slabs model (see inset figure in Fig. 5B) of the electron density profile (EDP, $\rho(z)$) normal to the interface with each slab of thickness d_i having a uniform density ρ_i [46]. The EDP provides a molecular scale view of the thickness of the interfacial layer. By integrating the EDP through the layer, the surface concentrations (Γ) can be obtained by accounting for the known number of electrons from all species at the interface and their partial molar volumes (see **Supplementary Information**). Errors in the fitted parameters are obtained by mapping the chi-square space (square deviation between the reflectivity measurement and fit for a given parameter set d_i, ρ_i and σ) which allows an assignment of the errors in the calculated surface concentrations.

Together with the XR, XFNTR is used to quantify Tb^{3+} in the adsorbed layers at the air/water interface (see **Methods**). These measurements are taken at angles near the critical value, α_c, for total external reflection, and the excitation through the layer and into the bulk liquid is in the form of an exponentially decaying wave passing through the interface. The spectrum of the fluorescence (see **Fig. S7**) is measured by a detector above the trough, and the integrated intensity of the strongest line of the Tb^{3+} fluorescence ($\mathcal{L}_\alpha$) is obtained for each of the values of Q_z near the critical angle. Fluorescence measurements from a solution without peptide and with a known concentration of cation are used to measure a calibration coefficient (see **Fig. S8**). The surface concentration of cations ($\Gamma_{Tb^{3+}}$) is then obtained by fitting the adsorbed species intensity as a function of Q_z with the calibration coefficient [40]; mapping of the error in the coefficient, as with the XR data, allows error bars to be assigned to the surface measurement [46]. With the cation surface concentration determined, the electron and molar volume balances are applied to calculate the surface concentrations of the peptide (see **Supplementary Information** for calculations).

The normalized reflectivity measurements ($\mathcal{R}/\mathcal{R}_F$ vs. Q_z) for interfacial layers adsorbed from solutions containing Tb^{3+}:peptide complexes and different concentrations of glutaraldehyde are given in Fig. 5A. As the concentration of glutaraldehyde in solution increases, the maximum value of $\mathcal{R}/\mathcal{R}_F$ shifts to lower Q_z and the appearance of a second peak is observed indicating the presence of a thicker interfacial layer. The electron density profiles, derived from the slab model fits, are given in Fig. 5B with fitting parameters given in **Table S1**.The construction of EDPs is useful for representing and determining thickness of interfacial layers and the distribution of the adsorbed molecules at the surface. As the interfacial film forms from non-networked Tb^{3+}:LBT^{3-} complexes, the layer from the solution containing 0.25 mM of GA have

thickness (approximately 14 Å). The thickness indicates only a monolayer coverage of Tb^{3+}:LBT^{3-} complexes, and the thickness agrees with MD simulations of these complexes at the air-water interface [20]. With concentrations of GA of 0.5 mM and higher, the presence of a thicker interfacial layer is observed with values of 37 Å for a bulk concentration of 0.5 mM of cross-linker, and 39 Å for both higher concentrations of GA (1 mM and 5 mM). These results indicate that for the peptide and Tb^{3+} bulk concentrations studied here, a bulk concentration of GA of 0.5 mM is necessary to induce the required cross-linking for the formation of Tb^{3+}-peptide-GA thicker layers at the air-water interface. Moreover, a maximum thickness (39 Å) is achieved with a GA concentration of 1 mM and further increasing the concentration of the cross-linker does not increase the thickness of the Tb^{3+}-LBT^{3-}-GA layer. It is important to note that although the GA-linked fibrils structures observed in solution have diameter of approximately 110 Å, the maximum thickness of films at the air-water interface is 1/3 of this value. This indicates that once these nano-structures are adsorbed to the air-water interface they most likely reorganize into a layer where hydrophobic interactions with air promote rearrangement and covalent bonds formed by glutaraldehyde are responsible for the thicker interfacial layer.

The surface concentrations of peptide reported in Fig. 5C, show that $\Gamma_{LBT^{3-}}$ increases with bulk concentration of glutaraldehyde, consistent with the observed reduction in surface tension and enhancement of the interfacial rheological properties of adsorbed layers when increasing the bulk concentration of the cross-linker. The independent XFNTR measurements of the surface concentration of Tb^{3+} with bulk concentration sufficient to saturate the peptide are given in Fig. 5D, with integrated fluorescence intensity and corresponding fits given in **Fig. S9**. As for the peptide, $\Gamma_{Tb^{3+}}$ increases with bulk concentration of glutaraldehyde (with ratios of LBT^{3-} to Tb^{3+} approximately 1).

The surface concentration of LBT^{3-} in the absence of trivalent cations and with GA at a bulk concentration of 1 mM was calculated from XR measurements ($\mathcal{R}/\mathcal{R}_F$ curve with fits and corresponding EPD are given in **Figs. S10A** and **S10B**, and the parameters for the slab model fit in **Table S2**). The unbound $\Gamma_{LBT^{3-}}$ (0.0035 ± 0.0002 molecules/Å^2), is approximately 31% of the $\Gamma_{LBT^{3-}}$ in the bound state (Tb^{3+}) at the same concentration of glutaraldehyde. This significant difference was unexpected because of the similarities between the quasi-equilibrium surface tension of the unbound LBT^{3-}-GA and the bound Tb^{3+}-LBT^{3-}-GA (see Fig. 3). However, this unexpected result can be attributed to the differences in the surface molecular arrangement and electrostatic interactions between the linked molecules (either unbound or Tb^{3+}-bound) populating the interface. While the interfacial surface might be saturated with LBT-GA linked conjugates, resulting in a quasi-equilibrium surface tension similar to a fully populated Tb^{3+}-LBT^{3-}-GA interface, the unbound peptide most likely has a more extended conformation. This extended conformation occupies a larger surface area than the bound peptide, leading to lower surface coverage of molecules. Moreover, the lower surface tension associated with a low surface coverage of unbound GA-linked peptides is the result of the electrostatic repulsion between negatively charged peptides at the air-water interface.

It is important to mention that the interfacial film formed by adsorbed unbound LBT-GA linked conjugates has a thickness of 18.8 ± 0.1 Å, representative of a single surface layer. Ultimately, the presence of a thicker interfacial layer (39.1 ± 0.3 Å, when bound with Tb^{3+} ions) has a negligible impact on surface tension values. Instead, the surface tensions are predominantly defined by the intermolecular interactions among the species populating the surface.

Surface concentration of LBT^{3-} in the absence of trivalent cations and with no GA was also calculated from XR measurements ($\mathcal{R}/\mathcal{R}_F$ curve with fits and corresponding EPD are given in **Figs. S10C** and **S10D**, and the parameters for the slab model fit in **Table S2**). This value, 0.0033 ± 0.0002 molecules/Å^2, shows that the surface concentration of uncomplexed peptide increases by only approximately 8% in the presence of glutaraldehyde. This indicates that while the peptides are linked, there is not a significant crowding of the surface that would enhance the rheological properties, as observed for the LBT^{3-}-Tb^{3+}-GA conjugates, and this is consistent with the reduction in dilational elasticity shown in **Fig. S5A**.

Competitive Adsorption of LBT^{3-}:Tb^{3+} and LBT^{3-}:La^{3+}. To gain insight into how the cross-linking of metal-peptide complexes induced by glutaraldehyde affects the surface selectivity for Tb^{3+} cations, solutions were prepared containing LBT^{3-} at a fixed concentration of 100 μM and GA at a fixed concentration of 1 mM and with a series of equimolar mixtures of Tb^{3+} and La^{3+}. The lighter cation lanthanum was chosen for the competitive analysis because in solution La^{3+} has less affinity than Tb^{3+} for the peptide (La^{3+} having a higher dissociation constant in solution phase, 19975 ± 70 nM, compared with Tb^{3+}, 656 ± 25 nM) [20]. Initially, XR and XFNTR measurements were taken for a layer from a solution containing 100 μM of LBT^{3-}, 400 μM of La^{3+} cations, and 1 mM of glutaraldehyde. **Fig. S11** provides the reflectivity, and fluorescence intensity with their respective fittings; and **Table S3** provides the slab model fitting parameters. The derived EDP from the XR data fitting shown in Fig. 6A (plotted along with the EDP of a layer from a solution containing 100 μM of LBT^{3-}, 400 μM of Tb^{3+}, and 1 mM of GA for comparison), indicates the presence of an interfacial layer of approximately 100 Å. This thicker film in the presence of La^{3+} results in a greater adsorption of peptide molecules and La^{3+} cations (see **Fig. S12**) compared with the film formed under the same conditions but with Tb^{3+} instead. The increased adsorption of molecules and ions at the interface, leading to a thicker layer, is likely due to enhanced cross-linking of La^{3+}:peptide complexes in solution by GA, since in the absence of the cross-linker LBT^{3-}:La^{3+} complexes at the bulk concentrations studied here form layers of similar thickness to those of Tb^{3+}-bound complexes [20]. **Fig. S13** shows that the resulting structures from the cross-linking of LBT^{3-}:La^{3+} complexes lack the well-ordered organization observed with Tb^{3+} binding. The loose and flexible assemblies originated from the La^{3+} binding may facilitate a higher degree of reaction between glutaraldehyde and a greater number of complexes, contrasting with the rigid and well-ordered assemblies formed by LBT^{3-}:Tb^{3+} complexes. TEM imaging of dry La^{3+}-LBT^{3-}-GA structures from a solution of 100 μM of peptide, 400 μM of cations, and 1 mM of the cross-linker is presented in Fig. 6C. These structures exhibit coral-like arrangements, as the uncrosslinked complexes, but with larger dimensions and interconnected assemblies. Note that the increased cross-linking resulted in increased turbidity of the sample and the formation of aggregates visible to the naked eye.

The surface concentration of LBT^{3-} peptide for the competitive study at 1 mM of GA (**Fig. S14A**) increases with increasing concentrations of total lanthanide concentration in solution. This trend is consistent with the measurements of quasi-equilibrium surface tension in the same solutions, where we observe surface tension slightly decreasing with increasing lanthanide concentration (see **Fig. S15A** for quasi-equilibrium surface tension, which are obtained from the data in **Fig. S15B**). XR profiles with fits are given in **Fig. S16** and corresponding EDP are presented in Fig. 6B. XFNTR integrated fluorescence intensities with fits are given in **Fig. S17**. The parameters for the slab model fit are given in **Table S4**. In contrast to observations for the uncrosslinked Tb^{3+}:LBT^{3-} complex [20], the glutaraldehyde-linked peptide $\Gamma_{LBT^{3-}}$ depends on the bulk concentration of lanthanides. This metal-dependency suggests that a significant increase in the surface adsorption of peptide and lanthanide is possible only when nearly total complexation of peptides with metals is achieved.

The ratio of Tb^{3+} to La^{3+} at the surface as a function of the total lanthanide cations to peptide concentration ratio is given in Fig. 6D, with surface concentrations of individual cations given in **Figs. S14B** and **S14C**. These values are plotted along the Tb^{3+}/La^{3+} surface concentration ratios of uncrosslinked complexes [20]. At low total concentration of cations in solution (< 300 μM), the surface coverage of La^{3+} is higher than Tb^{3+}, in agreement with the unlinked metal-peptide films (no glutaraldehyde in solution) and attributed to the higher surface activity of LBT^{3-}:La^{3+} over LBT^{3-}:Tb^{3+} complexes [20]. EDP from solutions containing equimolar mixtures of the two lanthanides show interfacial

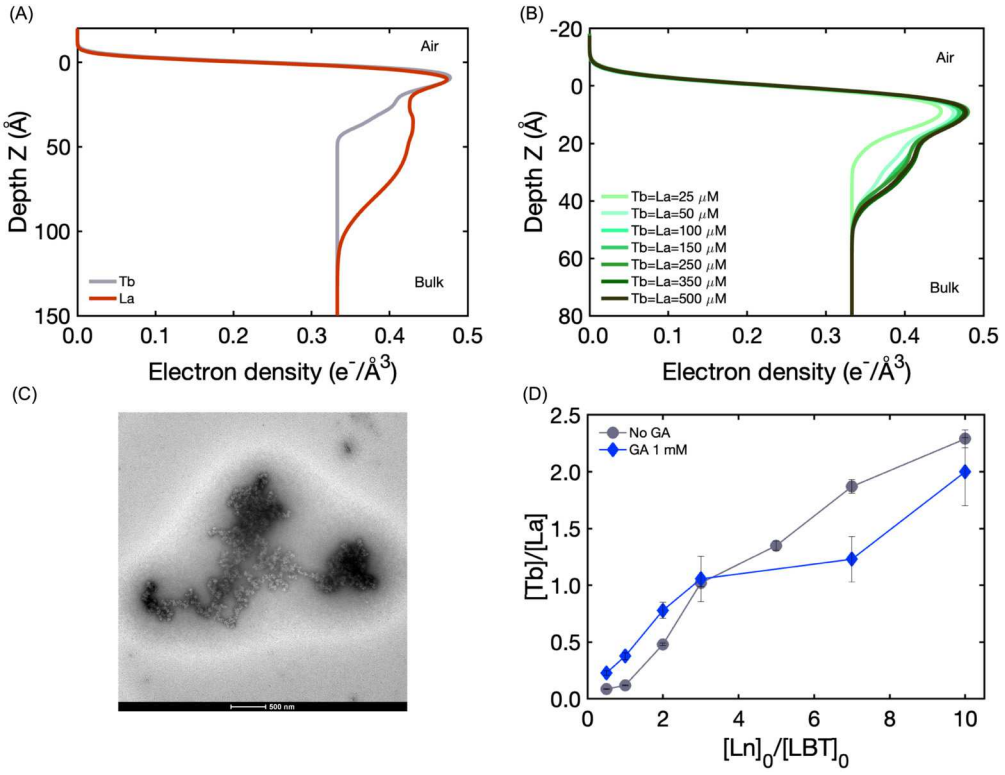

Fig. 6. (A) Electron density profiles from Parratt modeling for interfacial layers from solutions containing 100 μM of LBT^{3-}, 1 mM of GA, and either 400 μM of La^{3+} or 400 μM of Tb^{3+}. (B) Corresponding electron density profiles of the interfacial layers from Parratt modeling for surface films from solutions containing 100 μM of LBT^{3-}, 1 mM of GA, and different concentrations of lanthanides in an equimolar mixture of cations. (C) Dry TEM image from a solution containing 100 μM of LBT^{3-} peptide, 400 μM of La^{3+} cations and 1 mM of GA. (D) Ratio of total Tb^{3+} to La^{3+} at the interface for LBT^{3-} at 100 μM, GA 1 mM, and different concentrations of lanthanides in an equimolar mixture of cations (Tb^{3+}/La^{3+} ratios from complexes with no GA [20] are also reported for comparison).

layers with maximum thickness of 45 Å, which indicates that the concentration of Tb^{3+}:peptide complexes in solution is higher compared to that of the La^{3+}:peptide complexes (higher affinity for Tb^{3+} over La^{3+} remains). Supporting this assumption is the fact that La^{3+}-LBT^{3-}-GA linked conjugates adsorb to the air-water interface forming a 100 Å thick film. This type of film is not observed in any of the lanthanides mixtures solutions. Note that EDP of interfacial layer from the equimolar mixture of lanthanides at the lowest concentration (50 μM) shows the presence of a monolayer (see Fig. 6B), indicating that nearly total metal-complexation of the peptide is necessary for the formation of thicker layers at the air-water interface. This suggests that the complexed conformation of the peptide favors the cross-linking in solution and is consistent with the single layer observed for the films formed from a solution containing 100 μM of LBT^{3-} peptide with 1 mM of GA and no cations represented in **Fig. S10B**.

Finally, for high total concentration of lanthanide cations in solution (≥ 300 μM), the surface coverage of Tb^{3+} is higher than La^{3+}, with the Tb^{3+}/La^{3+} ratio increasing with total concentration of lanthanides in solution to a maximum value of 2.29 ± 0.08. This obtained surface ratio is consistent with the results obtained without GA in solution [20]. Moreover, we can infer that the results are not attributable to the glutaraldehyde cross-linking process. Instead, as for the uncrosslinked peptides, selective separation may be influenced by other factors such as structural alterations within the metal-peptide binding pocket upon adsorption to the air-water interface or during aggregation. Additionally, at low lanthanide concentrations, similar to the uncross-linked peptide [20], the higher surface density of La^{3+} can be attributed to the greater surface activity of La^{3+}-LBT^{3-}-GA linked conjugates compared to Tb^{3+}-LBT^{3-}-GA conjugates, as supported by quasi-equilibrium surface tension measurements (see **Fig. S18A**). This increased surface activity is further evidenced by the higher surface coverage observed with La^{3+}-peptide linked conjugates, which is 89% greater than that of Tb^{3+}-peptide linked conjugates (see Fig. 5C and **Fig. S12**).

It should be noted that while this difference in adsorption strength and surface activity between the linked metal-peptide conjugates can be leveraged in designing selective separation processes, the faster kinetics of La^{3+}-LBT^{3-}-GA might significantly influence the surface Tb^{3+}/La^{3+} ratios obtained in this study. Dynamic surface tension measurements (**Fig. S18B**) indicate that the initial drop in surface tension for La^{3+}-LBT^{3-}-GA conjugates occurs more rapidly than for Tb^{3+}-LBT^{3-}-GA, suggesting that La^{3+}-LBT^{3-} will dominate the interface first in an equimolar mixture of Tb^{3+} and La^{3+}, thereby affecting the initial stage of the surface separation of metals.

However, in a foam fractionation process, as the conjugates are gradually depleted and the concentration of La^{3+}-LBT^{3-}-GA decreases in solution, the separation is likely to favor the metal cation for which the peptide has a higher affinity (higher concentration of metal-peptide complexes). Although the affinity of the peptide may be influenced by the factors stated above, surface tension measurements and interfacial thickness data from XR analysis for solutions containing equimolar mixtures of Tb^{3+} and La^{3+} suggest a higher affinity of the peptide for Tb^{3+} over La^{3+}, as indicated by values closely matching those obtained from single-component studies involving Tb^{3+}. Further research is needed to fully understand two key aspects: (1) the selective adsorption of lanthanides using LBT peptides as extractants and (2) how to optimize or leverage the differences between bulk and surface affinity for a selective separation process of these metals. However, the adsorption ratios of Tb^{3+}/La^{3+} shown in Fig. 6D suggest that glutaraldehyde can serve as a cross-linker to enhance the adsorption of rare earth elements and stabilize surface films, all without altering the binding or affinity of individual metal-peptide complexes.

4. Conclusions

We have demonstrated that glutaraldehyde can cross-link lanthanide-LBT complexes and adsorb to air-water interfaces. This cross-linking increases the adsorption of peptide molecules and trivalent cations to the surface and enhances the rheological properties of the films formed at the interface. Moreover, the selective adsorption of lanthanides is not significantly modified upon cross-linking with glutaraldehyde. The improvement of the surface rheological properties of the films is engendered by the formation of thicker layers at the air-water interface, and this thicker layer only forms for glutaraldehyde cross-linked bound peptides in solution. The increase in the viscoelastic properties of the interfacial films was elucidated through detailed surface molecular characterization using x-ray measurements at the air-water interface, which revealed surface molecular density and the interfacial arrangement of lanthanide-LBT complexes.

These results support our hypothesis that glutaraldehyde can be used as a cross-linker to enhance the adsorption of lanthanide cations to air-water interfaces from bulk solution, showing a two-fold increase for Tb^{3+} ions. Additionally, glutaraldehyde cross-linking increases the dilational elastic modulus of peptide-lanthanide interfacial films by up to 98%, with E'' values comparable to those observed for stable foams in approaches using surfactants and polymers [47–49]. This cross-linking facilitates faster dynamic surface tension relaxation and the stable formation of thick interfacial films, optimal for maintaining foam stability [30–33].

This work provides a new strategy and simple method for the enhancement surface extraction of REEs and foam stability in a foam-based eco-friendly separation process. The results presented here are foundation for the future engineering of LBT peptides to improve the surface separation and surface selectivity of REEs. This can be achieved by tuning intermolecular interactions to promote or inhibit self-assembly and by applying the fundamental principles of interface science to control foam stability for reliable separation processes.

CRediT authorship contribution statement

Luis E. Ortuno Macias: Writing – original draft, Visualization, Validation, Software, Methodology, Investigation, Formal analysis, Data curation, Conceptualization. **Honghu Zhang:** Writing – review & editing, Software, Methodology. **Benjamin M. Ocko:** Writing – review & editing, Software, Methodology. **Kathleen J. Stebe:** Writing – review & editing, Resources, Investigation, Funding acquisition, Conceptualization. **Charles Maldarelli:** Writing – review & editing, Supervision, Resources, Investigation, Funding acquisition, Conceptualization. **Raymond S. Tu:** Writing – review & editing, Supervision, Resources, Investigation, Funding acquisition, Conceptualization.

Declaration of competing interest

The authors declare that they have no known competing financial interests or personal relationships that could have appeared to influence the work reported in this paper.

Data availability

No data was used for the research described in the article.

Acknowledgements

This work has been financially supported by the Department of Energy under the BES award No. DE-SC0022240. This research used the Open Platform Liquid Surfaces (OPLS) end station of the Soft Matter Interfaces Beamline (SMI, 12-ID) of the National Synchrotron Light Source II, a U.S. Department of Energy (DOE) Office of Science User Facility operated for the DOE Office of Science by Brookhaven National Laboratory under Contract No. DE-SC0012704. XModFit is developed at NSF's ChemMatCARS, Sector 15, which is supported by the Divisions of Chemistry (CHE) and Materials Research (DMR), National Science Foundation, under grant number NSF/CHE-1834750. Use of the Advanced Photon Source, an Office of Science User Facility operated for the U.S. Department of Energy (DOE) Office of Science by Argonne National Laboratory, was supported by the U.S. DOE under Contract No. DE-AC02-06CH11357.

Appendix A. Supplementary material

Supplementary material related to this article can be found online at https://doi.org/10.1016/j.jcis.2024.08.225.

References

[1] J. Zhang, B. Zhao, B. Schreiner, Separation Hydrometallurgy of Rare Earth Elements, Springer International Publishing, 2016.
[2] P. Cheng, Lanthanides: Fundamentals and Applications, Elsevier Science, 2023.
[3] K. Gschneidner, J. Bunzli, V. Pecharsky, Handbook on the Physics and Chemistry of Rare Earths, ISSN, Elsevier Science, 2010.
[4] M. Humphries, Rare Earth Elements: The Global Supply Chain, CRS Report for Congress, DIANE Publishing Company, 2010.
[5] R. Jyothi, Rare-Earth Metal Recovery for Green Technologies: Methods and Applications, Springer International Publishing, 2020.
[6] I. De Lima, W. Filho, Rare Earths Industry: Technological, Economic, and Environmental Implications, Elsevier Science, 2015.
[7] P. Lukac, M. Carboneras, P. Koltun, A. Tharumarajah, Life cycle impact of rare earth elements, ISRN Metall. 2014 (2014) 907536.
[8] V. Balaram, Rare earth elements: a review of applications, occurrence, exploration, analysis, recycling, and environmental impact, Geosci. Front. 10 (4) (2019) 1285–1303.
[9] K. Wang, H. Adidharma, M. Radosz, P. Wan, X. Xu, C.K. Russell, H. Tian, M. Fan, J. Yu, Recovery of rare earth elements with ionic liquids, Green Chem. 19 (2017) 4469–4493.
[10] V. Kaim, J. Rintala, C. He, Selective recovery of rare earth elements from e-waste via ionic liquid extraction: a review, Sep. Purif. Technol. 306 (2022) 122699.
[11] J. Zhang, J. Anawati, Y. Yao, G. Azimi, Aeriometallurgical extraction of rare earth elements from a ndfeb magnet utilizing supercritical fluids, ACS Sustain. Chem. Eng. 6 (12) (2018) 16713–16725.
[12] R. Shimizu, K. Sawada, Y. Enokida, I. Yamamoto, Supercritical fluid extraction of rare earth elements from luminescent material in waste fluorescent lamps, J. Supercrit. Fluids 33 (2005) 235–241.
[13] J. Wu, Z. Li, H. Tan, S. Du, T. Liu, Y. Yuan, X. Liu, H. Qiu, Highly selective separation of rare earth elements by zn-btc metal-organic framework/nanoporous graphene via in situ green synthesis, Anal. Chem. 93 (3) (2021) 1732–1739.
[14] X. Liang, Q. Zeng, Copolymers-functionalized metal-organic framework composite for efficient adsorption of rare-earth elements, Microporous Mesoporous Mater. 366 (2024) 112960.
[15] E. Elbashier, A. Mussa, M. Hafiz, A. Al Hawari, Recovery of rare earth elements from waste streams using membrane processes: an overview, Hydrometallurgy 204 (2021) 105706.
[16] L. Chen, Y. Wu, H. Dong, M. Meng, C. Li, Y. Yan, J. Chen, An overview on membrane strategies for rare earths extraction and separation, Sep. Purif. Technol. 197 (2018) 70–85.
[17] Z. Dong, J.A. Mattocks, G.J.P. Deblonde, D. Hu, Y. Jiao, J.A.J. Cotruvo, D.M. Park, Bridging hydrometallurgy and biochemistry: a protein-based process for recovery and separation of rare earth elements, ACS Cent. Sci. 7 (11) (2021) 1798–1808.
[18] T. Hatanaka, A. Matsugami, T. Nonaka, H. Takagi, F. Hayashi, T. Tani, N. Ishida, Rationally designed mineralization for selective recovery of the rare earth elements, Nat. Commun. 8 (1) (2017) 15670.
[19] L.J. Daumann, A natural lanthanide-binding protein facilitates separation and recovery of rare earth elements, ACS Cent. Sci. 7 (11) (2021) 1780–1782.
[20] L. Ortuno Macias, F. Jimenez-Angeles, J. Marmorstein, Y. Wang, S. Crane, S. KT, P. Sun, B. Sapkota, E. Hummingbird, W. Jung, B. Qiao, D. Lee, I. Dmochowski, R. Messinger, M. Schlossman, R. Radhakrishnan, E. Petersson, M. Cruz, W. Bu, C. Maldarelli, Lanthanide binding peptide surfactants at air-aqueous interfaces for interfacial separation of rare earth elements, ChemRxiv (2024).
[21] K.J. Franz, M. Nitz, B. Imperiali, Lanthanide-binding tags as versatile protein coexpression probes, ChemBioChem 4 (4) (2003) 265–271.
[22] M. Nitz, K.J. Franz, R.L. Maglathlin, B. Imperiali, A powerful combinatorial screen to identify high-affinity terbium(iii)-binding peptides, ChemBioChem 4 (4) (2003) 272–276.
[23] D.M. Park, D.W. Reed, M.C. Yung, A. Eslamimanesh, M.M. Lencka, A. Anderko, Y. Fujita, R.E. Riman, A. Navrotsky, Y. Jiao, Bioadsorption of rare earth elements through cell surface display of lanthanide binding tags, Environ. Sci. Technol. 50 (5) (2016) 2735–2742.

[24] X. Xie, X. Tan, Y. Yu, Y. Li, P. Wang, Y. Liang, Y. Yan, Effectively auto-regulated adsorption and recovery of rare earth elements via an engineered e. coli, J. Hazard. Mater. 424 (2022) 127642.
[25] D. Park, A. Middleton, R. Smith, G. Deblonde, D. Laudal, N. Theaker, H. Hsu-Kim, Y. Jiao, A biosorption-based approach for selective extraction of rare earth elements from coal byproducts, Sep. Purif. Technol. 241 (2020) 116726.
[26] A. Brewer, E. Chang, D.M. Park, T. Kou, Y. Li, L.N. Lammers, Y. Jiao, Recovery of rare earth elements from geothermal fluids through bacterial cell surface adsorption, Environ. Sci. Technol. 53 (13) (2019) 7714–7723.
[27] E. Chang, A.W. Brewer, D.M. Park, Y. Jiao, L.N. Lammers, Surface complexation model of rare earth element adsorption onto bacterial surfaces with lanthanide binding tags, Appl. Geochem. 112 (2020) 104478.
[28] P. Stevenson, X. Li, Foam Fractionation: Principles and Process Design, CRC Press, 2014.
[29] R. Prud'homme, Foams: Theory: Measurements: Applications, CRC Press, 2017.
[30] T. Tamura, Y. Kaneko, M. Ohyama, Dynamic surface tension and foaming properties of aqueous polyoxyethylene n-dodecyl ether solutions, J. Colloid Interface Sci. 173 (2) (1995) 493–499.
[31] D. Beneventi, B. Carre, A. Gandini, Role of surfactant structure on surface and foaming properties, Colloids Surf. A, Physicochem. Eng. Asp. 189 (1) (2001) 65–73.
[32] A.-L. Fameau, A. Salonen, Effect of particles and aggregated structures on the foam stability and aging, C. R. Phys. 15 (8) (2014) 748–760.
[33] G. Lin, J. Frostad, G. Fuller, Influence of interfacial elasticity on liquid entrainment in thin foam films, Phys. Rev. Fluids 3 (2018).
[34] D. Ekserova, D. Exerowa, G. Gochev, D. Platikanov, L. Liggieri, R. Miller, Foam Films and Foams: Fundamentals and Applications, Progress in Colloid and Interface Science, CRC Press, 2018.
[35] I. Migneault, C. Dartiguenave, M.J. Bertrand, K.C. Waldron, Glutaraldehyde: behavior in aqueous solution, reaction with proteins, and application to enzyme crosslinking, BioTechniques 37 (5) (2004) 790–796.
[36] N. Reddy, R. Reddy, Q. Jiang, Crosslinking biopolymers for biomedical applications, Trends Biotechnol. 33 (6) (2015) 362–369.
[37] F. Ravera, G. Loglio, V.I. Kovalchuk, Interfacial dilational rheology by oscillating bubble/drop methods, Curr. Opin. Colloid Interface Sci. 15 (4) (2010) 217–228.
[38] O. Soo-Gun, J.C. Slattery, Disk and biconical interfacial viscometers, J. Colloid Interface Sci. 67 (3) (1978) 516–525.
[39] P. Pershan, M. Schlossman, Liquid Surfaces and Interfaces: Synchrotron X-Ray Methods, Cambridge University Press, 2012.
[40] W. Bu, M. Mihaylov, D. Amoanu, B. Lin, M. Meron, I. Kuzmenko, L. Soderholm, M.L. Schlossman, X-ray studies of interfacial strontium-extractant complexes in a model solvent extraction system, J. Phys. Chem. B 118 (43) (2014) 12486–12500.
[41] W. Bu, H. Yu, G. Luo, M.K. Bera, B. Hou, A.W. Schuman, B. Lin, M. Meron, I. Kuzmenko, M.R. Antonio, L. Soderholm, M.L. Schlossman, Observation of a rare earth ion-extractant complex arrested at the oil-water interface during solvent extraction, J. Phys. Chem. B 118 (36) (2014) 10662–10674.
[42] J. Stendahl, M. Rao, M. Guler, S. Stupp, Intermolecular forces in the self-assembly of peptide amphiphile nanofibers, Adv. Funct. Mater. 16 (2006) 499–508.
[43] W. Ji, C. Yuan, S. Zilberzwige-Tal, R. Xing, P. Chakraborty, K. Tao, S. Gilead, X. Yan, E. Gazit, Metal-ion modulated structural transformation of amyloid-like dipeptide supramolecular self-assembly, ACS Nano 13 (6) (2019) 7300–7309.
[44] R. Zou, Q. Wang, J. Wu, J. Wu, C. Schmuck, H. Tian, Peptide self-assembly triggered by metal ions, Chem. Soc. Rev. 44 (2015) 5200–5219.
[45] S. Bochenek, A.A. Rudov, T. Sassmann, I.I. Potemkin, W. Richtering, Influence of architecture on the interfacial properties of polymers: linear chains, stars, and microgels, Langmuir 39 (50) (2023) 18354–18365.
[46] W. Bu, M. Bera, Xmodfit: X-ray modeling and fitting [online, cited 2023 December 1].
[47] H. Fauser, M. Uhlig, R. Miller, R. v. Klitzing, Surface adsorption of oppositely charged sds:c12tab mixtures and the relation to foam film formation and stability, J. Phys. Chem. B 119 (40) (2015) 12877–12886.
[48] H.-Q. Sun, L. Zhang, Z.-Q. Li, X.-W. Song, X.-L. Cao, L. Zhang, S. Zhao, J.-Y. Yu, Effect of alkyl chain length on the surface dilational rheological and foam properties of n-acyltaurate amphiphiles, Colloid Polym. Sci. 290 (1) (2012) 31–40.
[49] N. Kristen, A. Vüllings, A. Laschewsky, R. Miller, R. von Klitzing, Foam films from oppositely charged polyelectrolyte/surfactant mixtures: effect of polyelectrolyte and surfactant hydrophobicity on film stability, Langmuir 26 (12) (2010) 9321–9327.